

Supplementary material

Na₃[Ru₂(μ -CO₃)₄] as a homogeneous catalyst for water oxidation; HCO₃⁻ as a co-catalyst.

Shanti G. Patra, Totan Mondal, Sathiyam Krishnamoorthy, Amir Mizrahi, Haya Kornweitz, Dan Meyerstein

Materials

RuCl₃·3H₂O, NaClO₄·H₂O, NaHCO₃, Na₂CO₃ and H₂O₂ were purchased from Alfa Aesar. Ru₂(μ -CH₃COO)₄Cl[1] and Na₃[Ru₂(μ -CO₃)₄][2] were prepared following the literature procedure with slight modifications. All aqueous solutions of different concentrations were prepared from deionized water purified by a Millipore Milli-Q setup with a final resistivity of > 10 M Ω /cm.

Synthesis of Ru₂(μ -CH₃COO)₄Cl

RuCl₃·3H₂O (1.0 g) was taken in a mixture of glacial acetic acid (35 ml) and acetic anhydride (7.0 ml) under oxygen atmosphere and gently refluxed for 1.0 hr. In the course of reaction the initial brown colour changes to dark green. The black residue formed after ~ 1 hr was removed by filtration after cooling. The solution was then further refluxed for another 10 hrs, by that time the solution colour changes to emerald-green in colour. The reddish-brown microcrystalline compound formed was filtered after cooling then washed by small amounts of acetic acid, methanol and diethyl ether and dried.

Synthesis of Na₃[Ru₂(μ -CO₃)₄]

Ru₂(μ -CH₃COO)₄Cl (0.25 g, 0.52 mmol) was suspended in 10 ml aqueous solution of Na₂CO₃ (0.38 g, 3.16 mmol). The reaction mixture was then refluxed for 2.0 hrs under N₂ atmosphere. The black precipitate formed was removed by filtration without cooling and to the filtrate acetone was added drop wise with stirring until an orange precipitate started to form. The precipitate formed was filtered, washed with diethyl ether and dried. The formation of the desired product was confirmed by UV-Vis spectra, $\lambda = 337$ nm ($\epsilon = 336$ dm³ mol⁻¹ cm⁻¹) and 412 nm ($\epsilon = 834$ dm³ mol⁻¹ cm⁻¹).

Instrumentation and measurements

Scanning electron microscopy (SEM) studies were performed using a TESCAN MAIA3 instrument. To determine the composition, energy dispersive X-ray analyses in SEM mode (SEMEDX) were performed using the Aztec materials characterization system. UV-vis spectra were measured using an Agilent 8453 diode-array spectrophotometer. pH values were measured using SCHOTT 850 benchtop pH meter using a pH electrode from SI Analytical, GmbH.

Glassy carbon (0.071 cm²) disk electrode pre-treatment

Before the electrochemical measurements the glassy carbon working electrode was first polished with 1 μm Al₂O₃ to remove any deposited material followed by polishing with 0.05 μm Al₂O₃ to make the surface smooth. Then it was sonicated in water using an ultrasonic bath for 30 s to remove any particles from the surface. Finally, 30 cycles of CVs were performed in 0.50 M H₂SO₄ to clean it electrochemically.

Determination of diffusion coefficient (*D*)

The diffusion coefficient of a species was obtained by using the Randles-Sevcik equation. The relationship between the peak current density, i_p and the diffusion coefficient of the oxidized species, D , is as follows:

$$i_p = 0.496n_d \alpha^{1/2} F A C \left(\frac{n_d F \nu D}{RT} \right)^{1/2}$$

where, i_p is the peak current density in A, D is the diffusion coefficient of the specie in cm²s⁻¹, C is the bulk concentration of oxidative species mol cm⁻³, ν is scan rate in V·s⁻¹. One can calculate the D from the slope of the i_p vs. $\nu^{1/2}$ plot.

Determination of standard rate constant (k_0)

The standard rate constant, k_0 , was obtained by using the Nicholson method[3]. For an electron transfer process (oxidation) the relation between standard rate constant and the Nicholson dimensionless parameter, ψ is given by the following equation:

$$k_0 = \left[\frac{(\pi \cdot D_R \cdot f \cdot \nu)^{1/2}}{(D_R/D_O)^{\alpha/2}} \right] \psi$$

k_0 is the standard rate constant in cm^2s^{-1} ; π is the mathematical constant; ψ is the Nicolson dimensionless number, which is obtained from peak potential separation (ΔE_p) from CV curve.

D_O and D_R are the diffusion coefficient of oxidizing specie and reducing specie respectively in cm^2s^{-1} ; and v is scan rate in Vs^{-1} ; α is the charge transfer coefficient, dimensionless; and $f = (n \cdot F)/(R \cdot T)$, in which n is the number of electrons transferred in the redox reaction, F is the Faraday constant ($96485 \text{ C}\cdot\text{mol}^{-1}$), R is the ideal gas constant ($8.314 \text{ J}\cdot\text{mol}^{-1}\cdot\text{K}^{-1}$), T is the absolute temperature in K.

Computational details

A hybrid functional, Becke's three-parameter Lee-Yang-Parr (B3LYP), was used for geometry optimization using the density functional theory (DFT) method implemented in the Gaussian16 quantum chemistry software. The Pople's basis set 6-311+G(d,p) is utilized for all the non-metal atoms, whereas the well-established Stuttgart/Dresden (SDD) basis set with the effective core potential (ECP) was exploited for Ru. In addition, the dispersion effect was imposed using the Grimme D3 correction with Becke-Johnson damping (BJ) during geometry minimization. The vibration frequency analyses were performed at the same theoretical level to ensure the real minima ($N_{\text{img}} = 0$) and to obtain the thermodynamic energy corrections. The hydration effect was considered by a self-consistent reaction field (SCRF) approach using Truler's SMD model with default parameters for water. In solution, most of the species were defined by 1 (M) standard state, and 55.5 (M) was considered for water. Therefore, for other concentrations (C), additional corrections were made according to the following equation: $RT \ln(C)$. The exact calculation of a proton free energy in solution is not straight forward, and thus, we adopted a value of -272.20 kcal/mol . NBO analysis implemented in Gaussian16 is used to calculate partial charges and Wiberg indices, which are a measure of bond orders. In order to compare the excitation energies obtained from the experimental UV-vis spectra, TD-DFT calculation was performed utilizing long-range corrected hybrid CAM-B3LYP functional. The 3D images of the optimized structures were captured using CYLview visualization software. Unless explicitly stated, all reported energies are the Gibbs free energies in kcal/mol.

References

- [1] T.. Stephenson, G. Wilkinson, New ruthenium carboxylate complexes, *J. Inorg. Nucl. Chem.* 28 (1966) 2285–2291. doi:10.1016/0022-1902(66)80118-5.
- [2] F.A. Cotton, L. Labella, M. Shang, Further study of tetracarbonato diruthenium(II,III) compounds, *Inorg. Chem.* 31 (1992) 2385–2389. doi:10.1021/ic00038a017.
- [3] R.S. Nicholson, Theory and Application of Cyclic Voltammetry for Measurement of Electrode Reaction Kinetics, *Anal. Chem.* 37 (1965) 1351–1355. doi:10.1021/ac60230a016.

Table S1

The values of anodic peak (E_{pa} (V)) and cathodic (E_{pc} (V)) peak potential, their difference, ΔE_p (V); Nicholson parameter, ψ and rate constant of electron transfer, k_0 (cm s^{-1}) at different scan rate (V s^{-1}) for the redox couple $\text{Ru}^{\text{III}}\text{Ru}^{\text{III}}/\text{Ru}^{\text{III}}\text{Ru}^{\text{II}}$ in neutral medium.^a

| ν | E_{pa} | E_{pc} | ΔE_p | $\ln(\psi)$ | ψ | $k_0 \times 10^3$ |
|-------|----------|----------|--------------|-------------|--------|-------------------|
| 0.005 | 0.870 | 0.792 | 0.078 | 0.258 | 1.194 | 1.091 |
| 0.010 | 0.876 | 0.789 | 0.087 | -0.145 | 1.030 | 1.030 |
| 0.020 | 0.882 | 0.786 | 0.096 | -0.445 | 1.081 | 1.081 |
| 0.050 | 0.890 | 0.783 | 0.107 | -0.759 | 1.246 | 1.246 |
| 0.100 | 0.894 | 0.776 | 0.118 | -1.009 | 1.371 | 1.371 |
| 0.200 | 0.906 | 0.770 | 0.136 | -1.337 | 1.401 | 1.401 |
| 0.300 | 0.926 | 0.765 | 0.161 | -1.752 | 1.285 | 1.285 |
| 0.400 | 0.941 | 0.759 | 0.182 | -1.977 | 1.039 | 1.039 |
| 0.500 | 0.956 | 0.756 | 0.196 | -2.117 | 1.011 | 1.010 |

^a The average value of k_0 is $(1.15 \pm 0.15) \times 10^{-3} \text{ cm s}^{-1}$.

Table S2

The values of E_{pa} (V), E_{pc} (V), ΔE_p (V), ψ and k_0 (cm s^{-1}) at different scan rate (V s^{-1}) for the redox couple $\text{Ru}^{\text{IV}}\text{Ru}^{\text{V}}/\text{Ru}^{\text{IV}}\text{Ru}^{\text{IV}}$ in bicarbonate medium.^a

| ν | E_{pa} | E_{pc} | ΔE_p | $\ln(\psi)$ | ψ | $k_0 \times 10^3$ |
|-------|----------|----------|--------------|-------------|--------|-------------------|
| 0.010 | 1.000 | 0.915 | 0.085 | -0.048 | 0.953 | 2.099 |
| 0.020 | 1.007 | 0.907 | 0.100 | -0.583 | 0.558 | 1.738 |
| 0.050 | 1.029 | 0.905 | 0.124 | -1.119 | 0.327 | 1.611 |
| 0.100 | 1.046 | 0.901 | 0.145 | -1.459 | 0.233 | 1.623 |
| 0.200 | 1.053 | 0.888 | 0.165 | -1.838 | 0.159 | 1.566 |
| 0.300 | 1.066 | 0.881 | 0.185 | -2.046 | 0.129 | 1.556 |
| 0.400 | 1.076 | 0.874 | 0.202 | -2.222 | 0.108 | 1.505 |
| 0.500 | 1.103 | 0.869 | 0.234 | -2.238 | 0.092 | 1.432 |

^a The average value of k_0 is $(1.57 \pm 0.05) \times 10^{-3} \text{ cm s}^{-1}$ (1st value has not been considered for averaging).

Table S3

The values of E_{pa} (V), E_{pc} (V), ΔE_p (V), ψ and k_0 (cm s^{-1}) at different scan rate (V s^{-1}) for the redox couple for the redox couple $\text{Ru}^{\text{II}}\text{Ru}^{\text{III}}/\text{Ru}^{\text{II}}\text{Ru}^{\text{II}}$ in bicarbonate medium.^a

| ν | E_{pa} | E_{pc} | ΔE_p | $\ln(\psi)$ | ψ | $k_0 \times 10^3$ |
|-------|----------|----------|--------------|-------------|--------|-------------------|
| 0.005 | -0.718 | -0.647 | 0.071 | 0.767 | 2.153 | 2.735 |
| 0.010 | -0.720 | -0.645 | 0.075 | 0.452 | 1.571 | 2.823 |
| 0.020 | -0.725 | -0.643 | 0.082 | 0.077 | 1.080 | 2.744 |
| 0.050 | -0.729 | -0.638 | 0.091 | -0.270 | 0.763 | 3.066 |
| 0.100 | -0.734 | -0.635 | 0.099 | -0.551 | 0.576 | 3.273 |
| 0.200 | -0.741 | -0.630 | 0.111 | -0.846 | 0.429 | 3.447 |
| 0.300 | -0.745 | -0.625 | 0.120 | -1.033 | 0.356 | 3.504 |
| 0.400 | -0.752 | -0.623 | 0.129 | -1.221 | 0.295 | 3.353 |
| 0.500 | -0.759 | -0.618 | 0.141 | -1.395 | 0.248 | 3.151 |

^a The average value of k_0 is $(3.12 \pm 0.30) \times 10^{-3} \text{ cm s}^{-1}$.

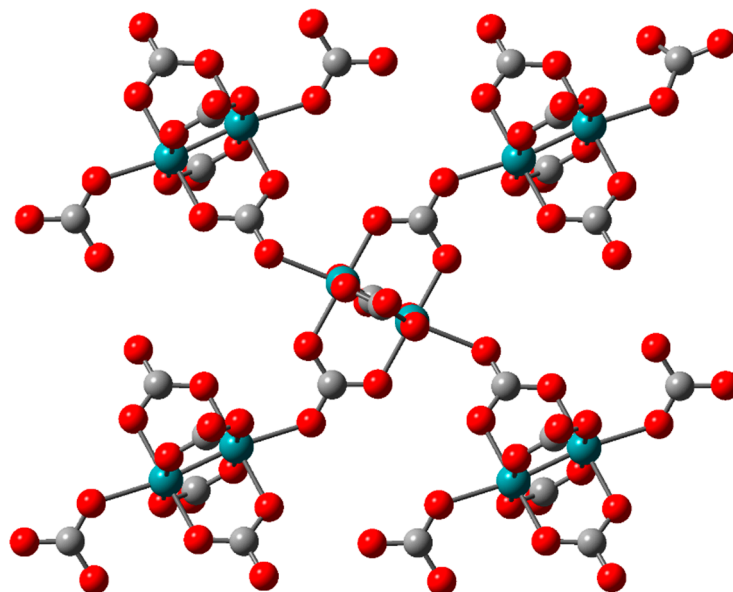


Figure S1. The crystal structure of $\text{Na}_3[\text{Ru}(\mu\text{-CO}_3)_4]$ showing the axial coordination of carbonate ligand from another complex. CCDC No. 1200939.

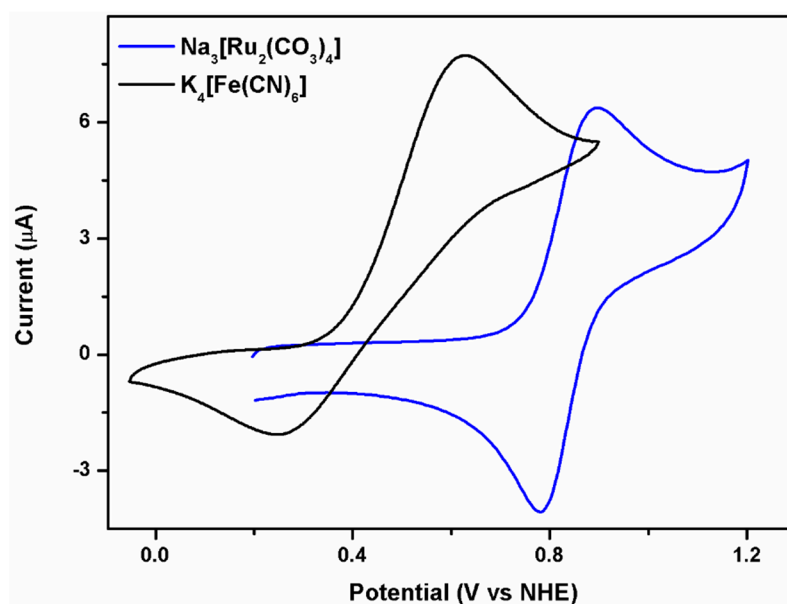


Figure S2. CVs of 1.0 mM $\text{Na}_3[\text{Ru}_2(\mu\text{-CO}_3)_4]$ in 0.20 M NaClO_4 (pH 7.0) and 1 mM $\text{K}_4[\text{Fe}(\text{CN})_6]$ and 0.20 M NaClO_4 at a scan rate of $50 \text{ mV}\cdot\text{s}^{-1}$.

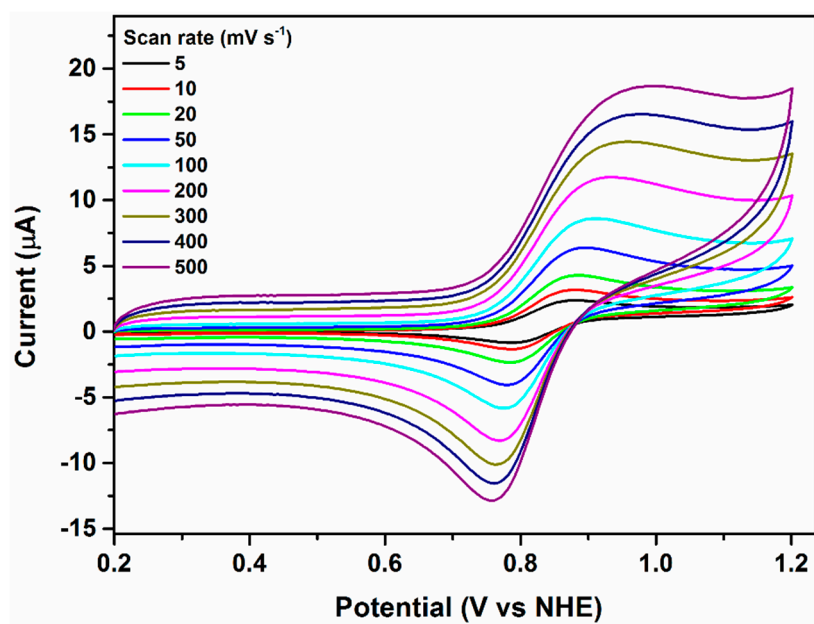


Figure S3. CVs of 1.0 mM $\text{Na}_3[\text{Ru}_2(\mu\text{-CO}_3)_4]$ in 0.20 M NaClO_4 (pH 7.0) at various scan rates.

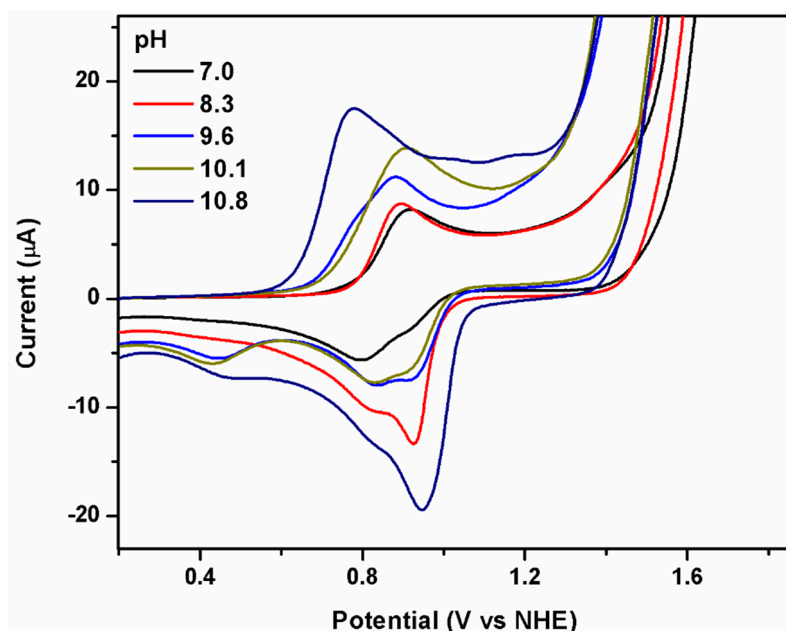


Figure S4. CVs of 1.0 mM $\text{Na}_3[\text{Ru}_2(\mu\text{-CO}_3)_4]$ in 0.20 M NaClO_4 solution at different pHs with a scan rate of $50 \text{ mV}\cdot\text{s}^{-1}$ highlighting the first redox couple.

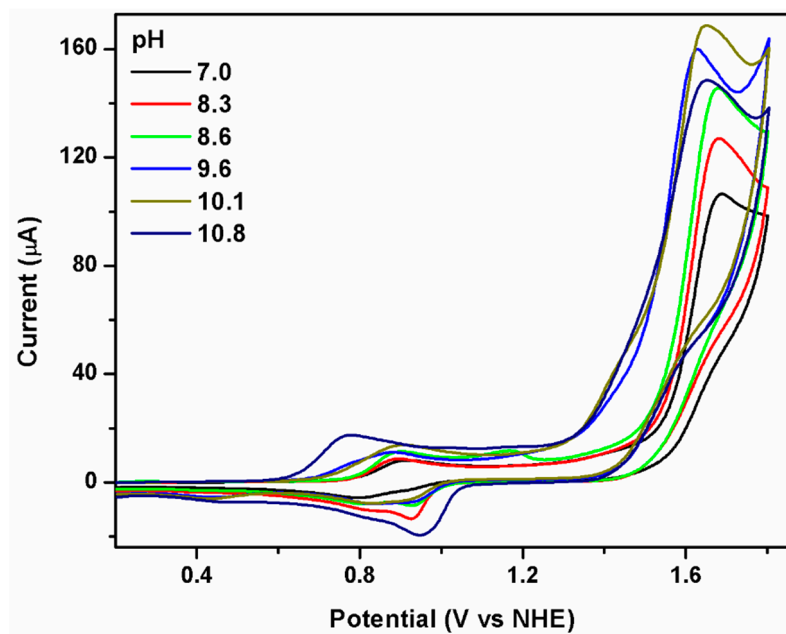


Figure S5. CVs of 1.0 mM $\text{Na}_3[\text{Ru}_2(\mu\text{-CO}_3)_4]$ in 0.20 M NaClO_4 solution at different pHs with a scan rate of $50 \text{ mV}\cdot\text{s}^{-1}$.

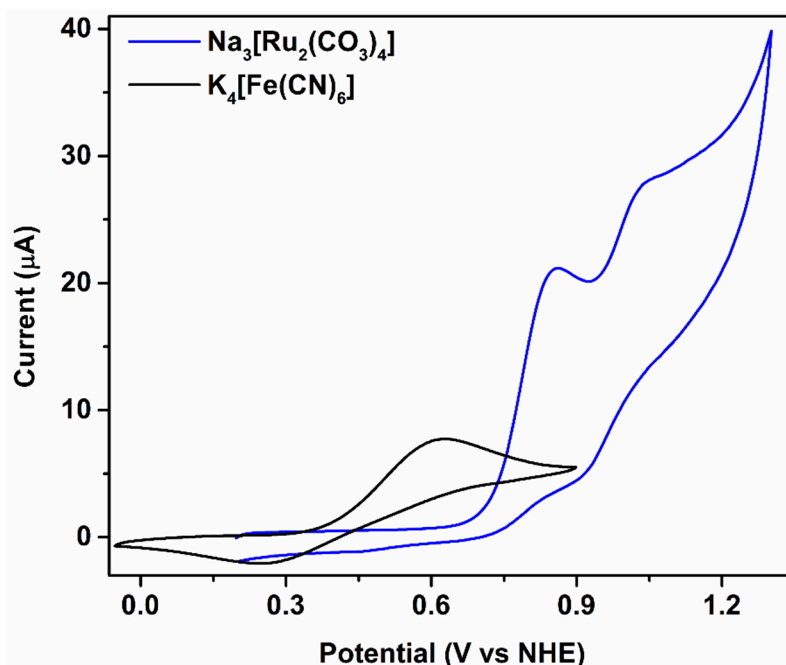


Figure S6. CVs of 1.0 mM $\text{Na}_3[\text{Ru}_2(\mu\text{-CO}_3)_4]$ and 1.0 mM $\text{K}_4[\text{Fe}(\text{CN})_6]$ in 0.10 M NaHCO_3 (pH 8.3) at a scan rate of $50 \text{ mV}\cdot\text{s}^{-1}$.

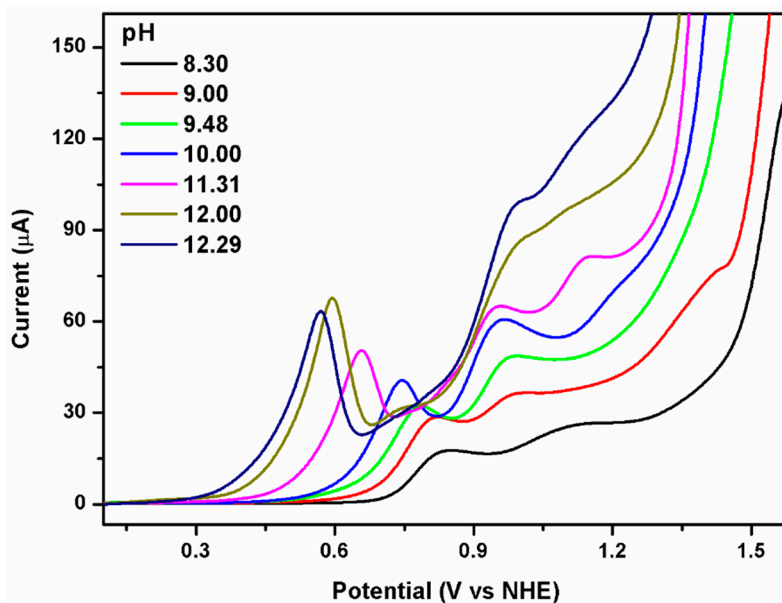


Figure S7. CVs of 1.0 mM $\text{Na}_3[\text{Ru}_2(\mu\text{-CO}_3)_4]$ in 0.10 M NaHCO_3 solution at different pHs with a scan rate of $50 \text{ mV}\cdot\text{s}^{-1}$.

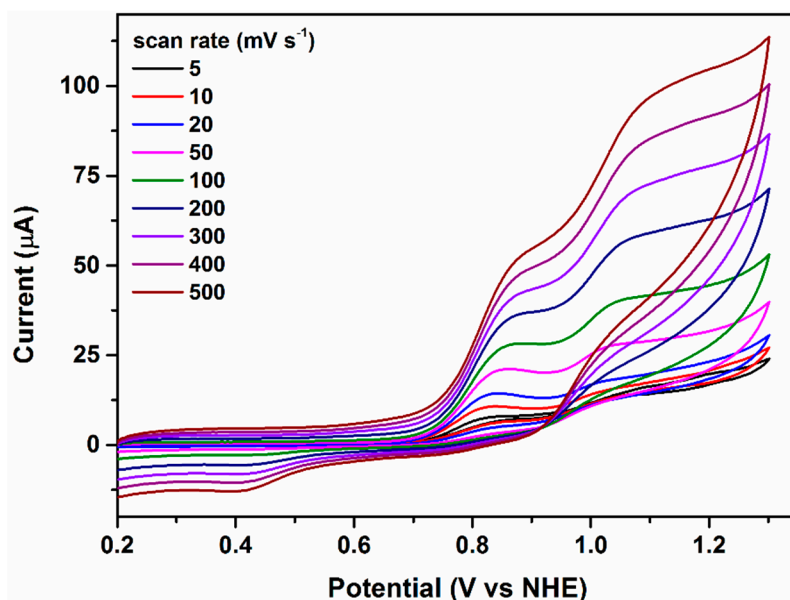


Figure S8. CVs of 1.0 mM $\text{Na}_3[\text{Ru}_2(\mu\text{-CO}_3)_4]$ in 0.10 M NaHCO_3 (pH 8.3) at various scan rates highlighting the first two redox processes.

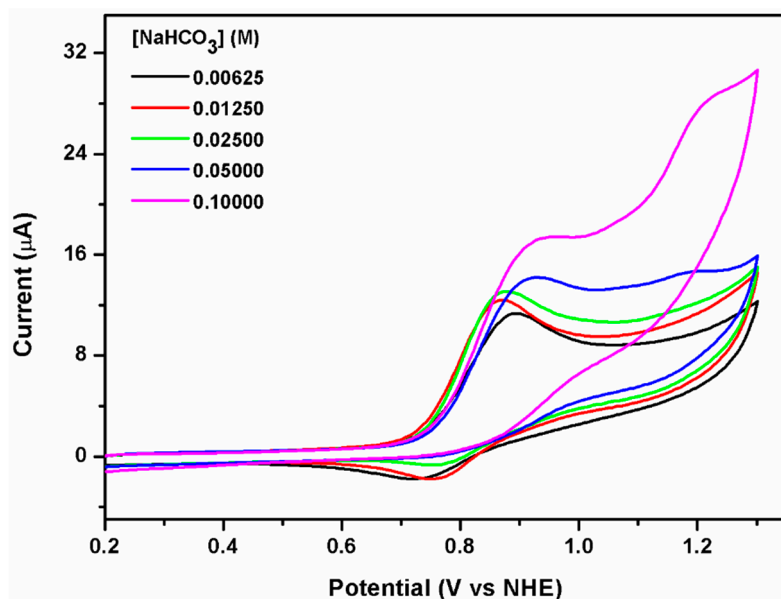


Figure S9. CVs of increasing concentrations of NaHCO_3 (pH 8.3) in 1.0 mM $\text{Na}_3[\text{Ru}_2(\mu\text{-CO}_3)_4]$ with a scan rate of $50 \text{ mV}\cdot\text{s}^{-1}$ highlighting the $\text{Ru}^{\text{III}}\text{Ru}^{\text{III}}/\text{Ru}^{\text{III}}\text{Ru}^{\text{II}}$ redox couple.

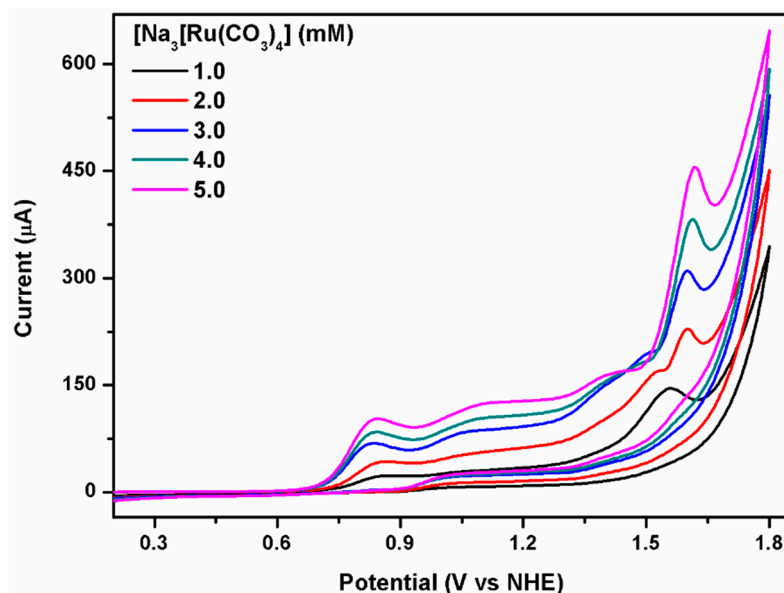


Figure S10. CVs of increasing concentrations of $\text{Na}_3[\text{Ru}_2(\mu\text{-CO}_3)_4]$ in 0.10 M NaHCO_3 (pH 8.3) with a scan rate of $50 \text{ mV}\cdot\text{s}^{-1}$.

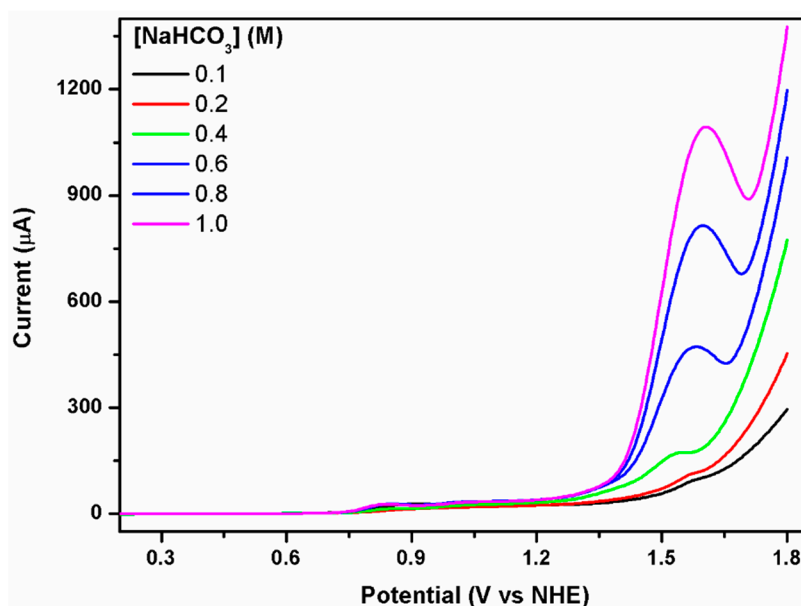


Figure S11. CVs of increasing concentrations of NaHCO_3 (pH 8.3) in 1.0 mM $\text{Na}_3[\text{Ru}_2(\mu\text{-CO}_3)_4]$ with a scan rate of $50 \text{ mV}\cdot\text{s}^{-1}$.

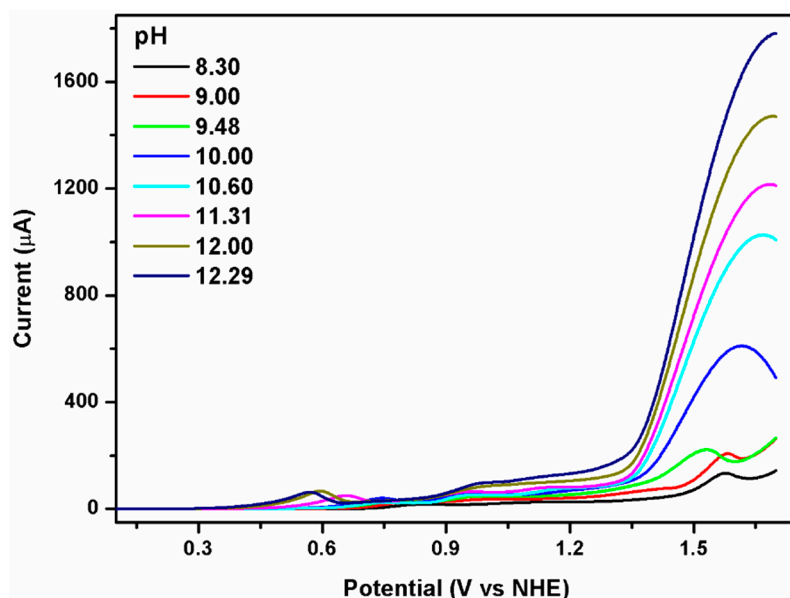


Figure S12. The CVs of 1.0 mM $\text{Na}_3[\text{Ru}_2(\mu\text{-CO}_3)_4]$ in 0.19 M NaHCO_3 at various pHs with a scan rate of 50 mV s^{-1} .

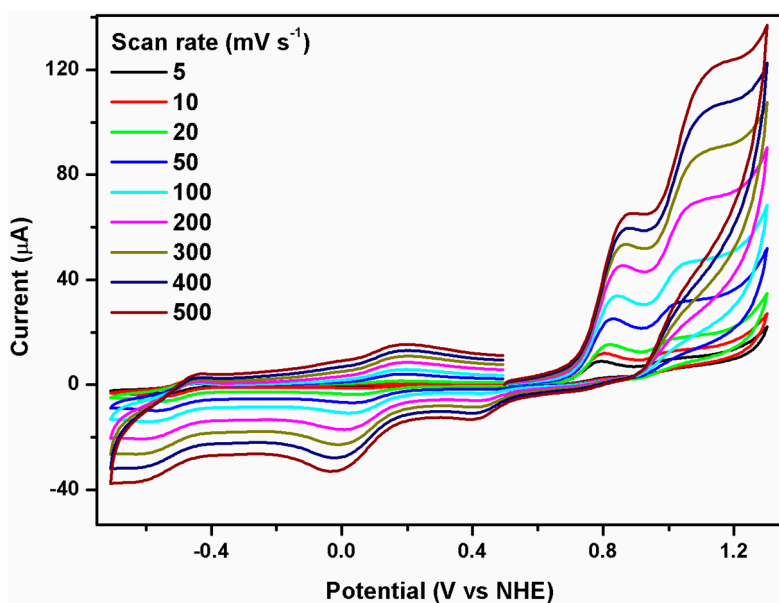


Figure S13. CVs of 1.0 mM $\text{Na}_3[\text{Ru}_2(\mu\text{-CO}_3)_4]$ in 0.10 M NaHCO_3 (pH 8.3) at various scan rates.

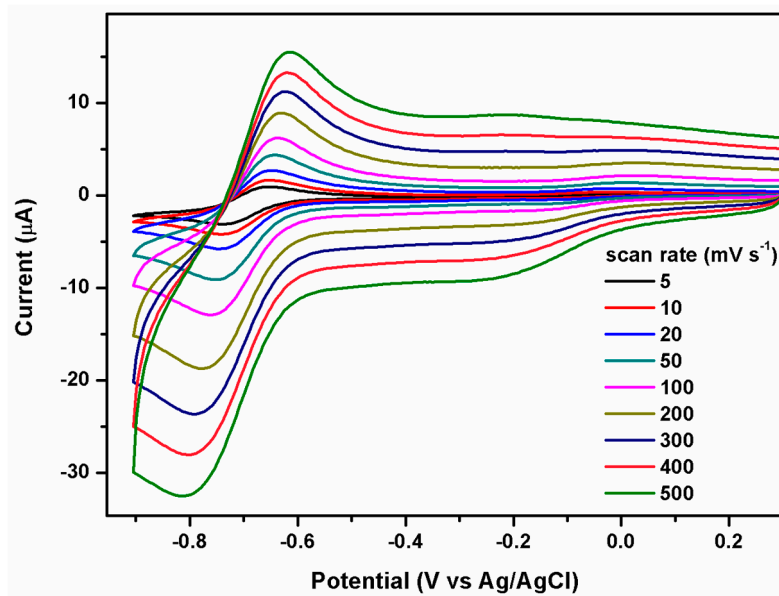


Figure S14. CVs of 1.0 mM $\text{Na}_3[\text{Ru}_2(\mu\text{-CO}_3)_4]$ in 0.10 M NaHCO_3 (pH 8.3) at various scan rates.

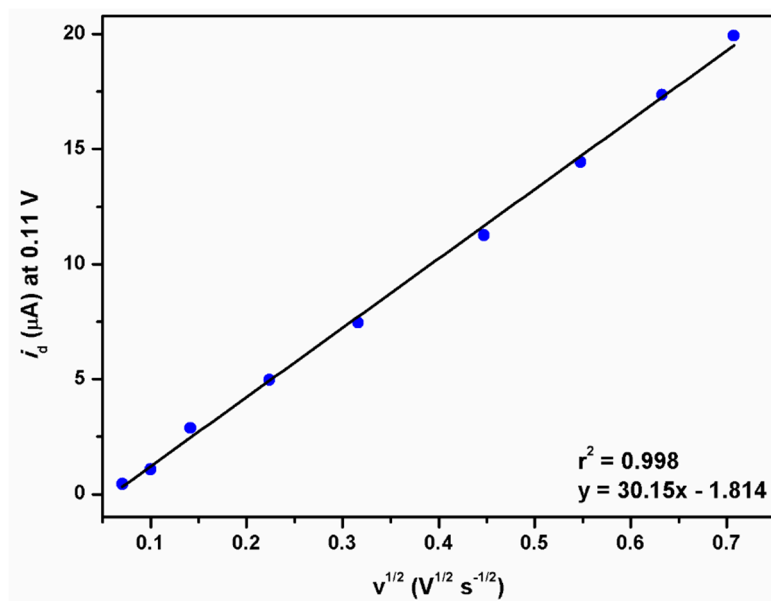


Figure S15. i_d at E_{pc} of 0.11 V vs. $v^{1/2}$ in 1.0 mM $Na_3[Ru_2(\mu-CO_3)_4]$ and 0.10 M $NaHCO_3$ (pH 8.3).

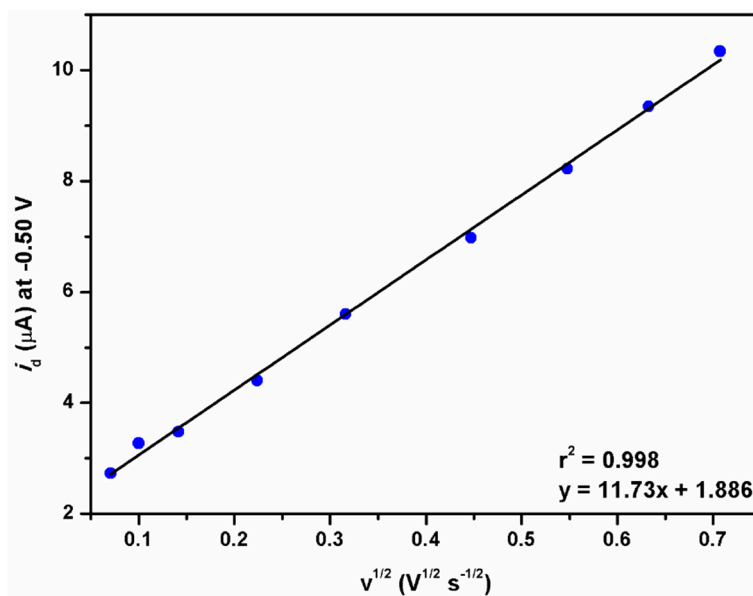


Figure S16. i_d at E_{pc} of -0.50 V vs. $v^{1/2}$ in 1.0 mM $Na_3[Ru_2(\mu-CO_3)_4]$ and 0.10 M $NaHCO_3$ (pH 8.3).

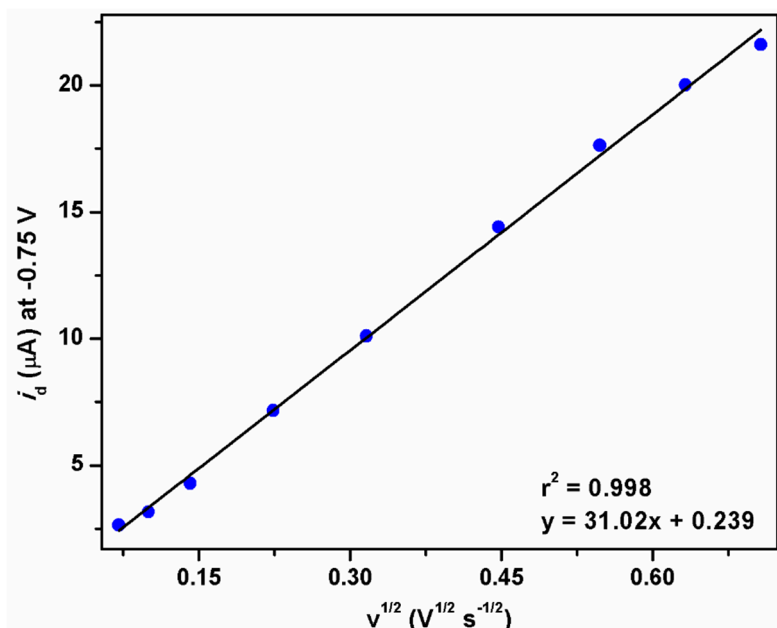


Figure S17. i_d at E_{pc} of -0.75 V vs. $v^{1/2}$ in 1.0 mM $\text{Na}_3[\text{Ru}_2(\mu\text{-CO}_3)_4]$ and 0.10 M NaHCO_3 (pH 8.3).

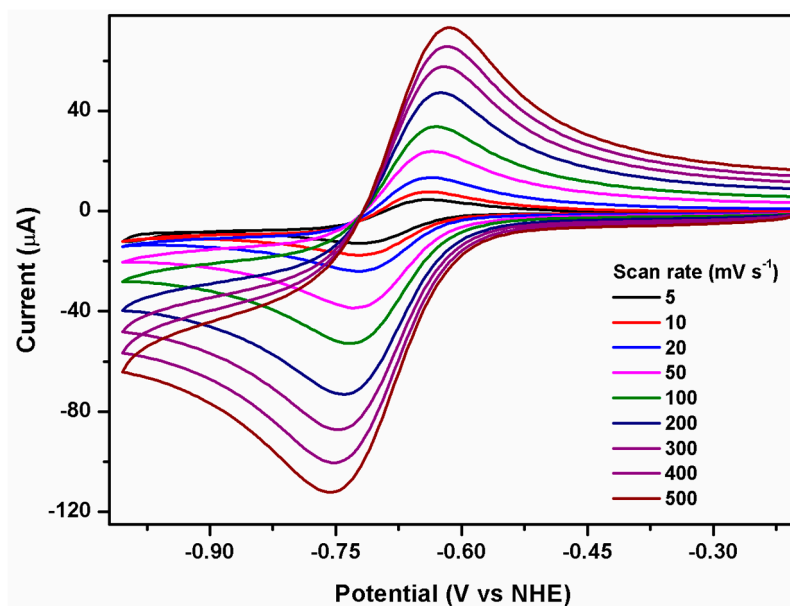


Figure S18. CVs of 5.0 mM $\text{Na}_3[\text{Ru}_2(\mu\text{-CO}_3)_4]$ in 0.10 M NaHCO_3 (pH 8.3) highlighting the $\text{Ru}^{\text{III}}\text{Ru}^{\text{II}}/\text{Ru}^{\text{II}}\text{Ru}^{\text{II}}$ couple.

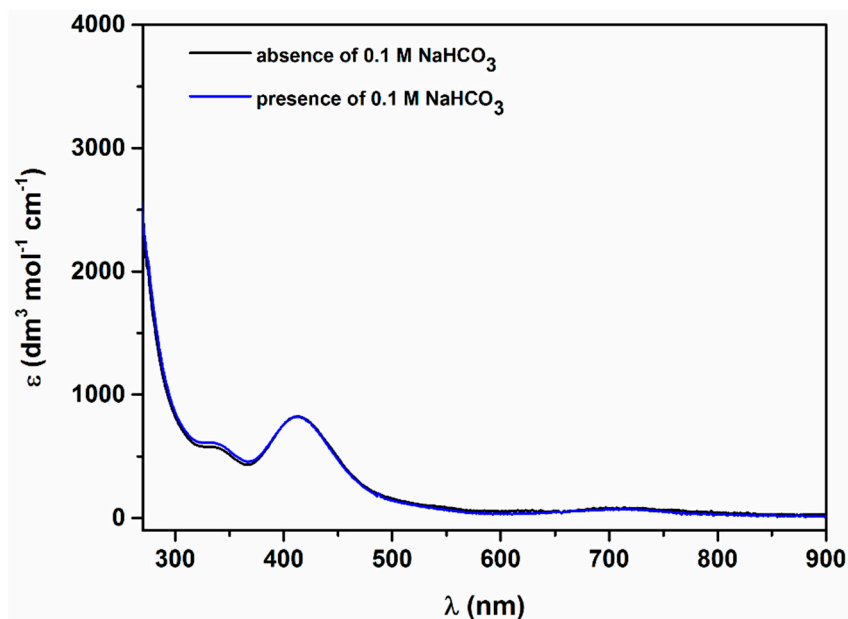


Figure S19. Absorption spectra of 1.0 mM $\text{Na}_3[\text{Ru}_2(\mu\text{-CO}_3)_4]$ in presence and absence of 0.10 M NaHCO_3 .

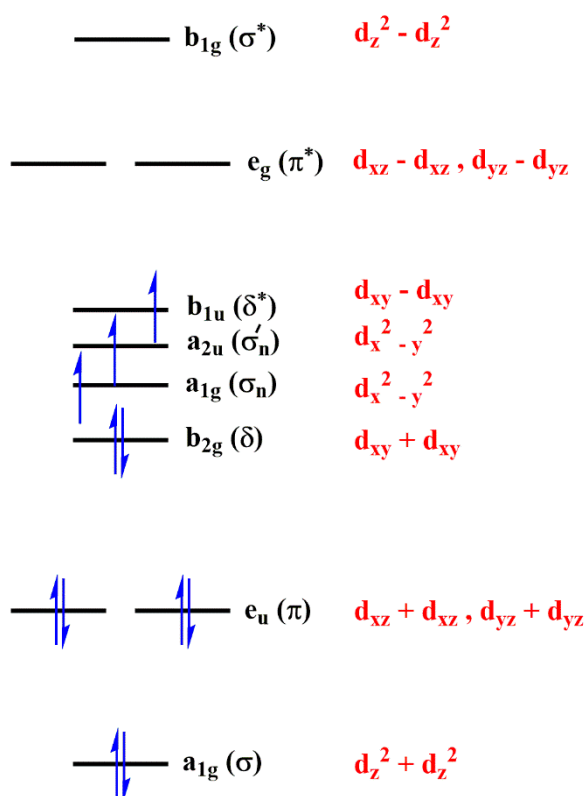


Figure 20. A qualitative MO diagram of the metal-metal bonding for an M_2X_8 (M = transition metal and X is halide) species of symmetry D_{4h} . The electron distribution shown is that for $[\text{Ru}_2(\mu\text{-CO}_3)_4]^{3+}$.

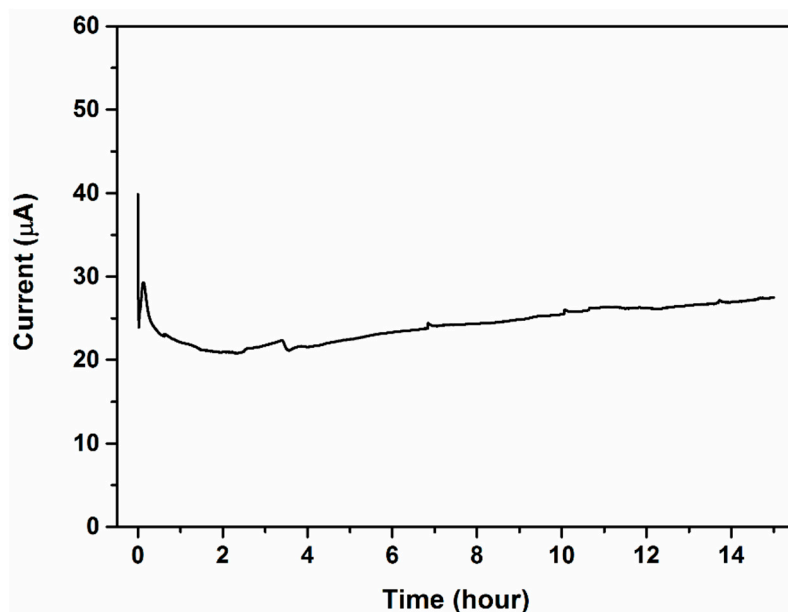


Figure S21. The chronoamperometry (CA) of 1.0 mM $\text{Na}_3[\text{Ru}_2(\mu\text{-CO}_3)_4]$ in 0.10 M NaHCO_3 at pH 8.3 for 15 hours at a potential of 1.6 V vs. NHE.

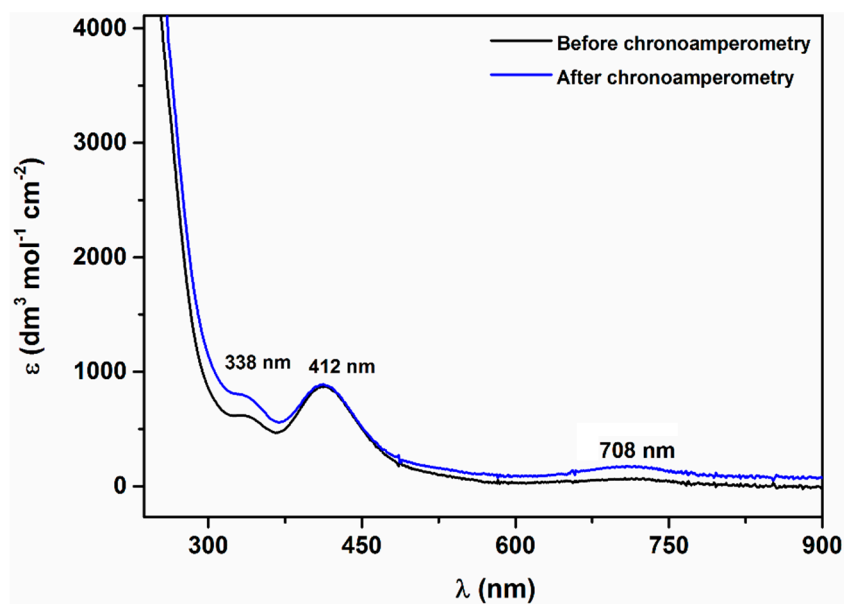


Figure S22. Absorption spectra before and after CA of a solution containing 1.0 mM $\text{Na}_3[\text{Ru}_2(\mu\text{-CO}_3)_4]$, 0.10 M NaHCO_3 at 1.6 V vs. NHE for 15 hours.

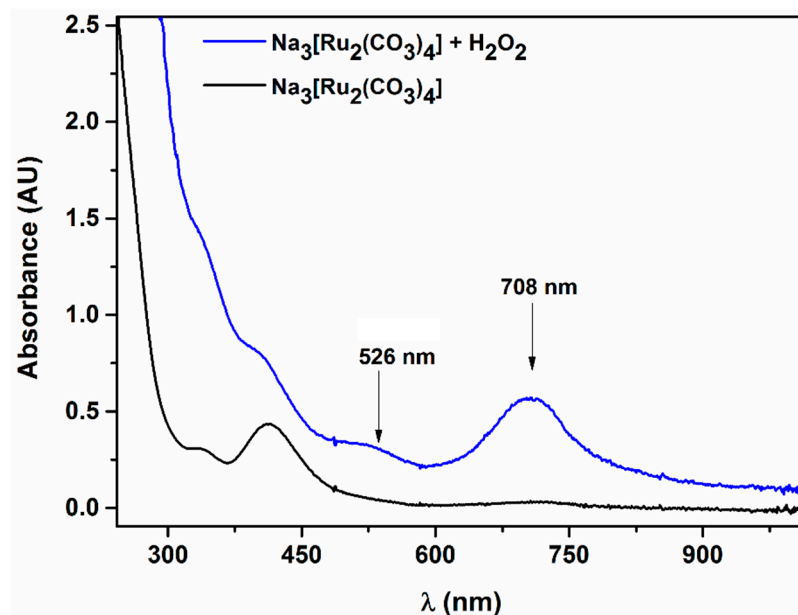


Figure S23. Absorption spectra before and after CA of a solution containing 1.0 mM $\text{Na}_3[\text{Ru}_2(\mu\text{-CO}_3)_4]$, 0.10 M NaHCO_3 at 1.6 V vs. NHE for 15 hours.

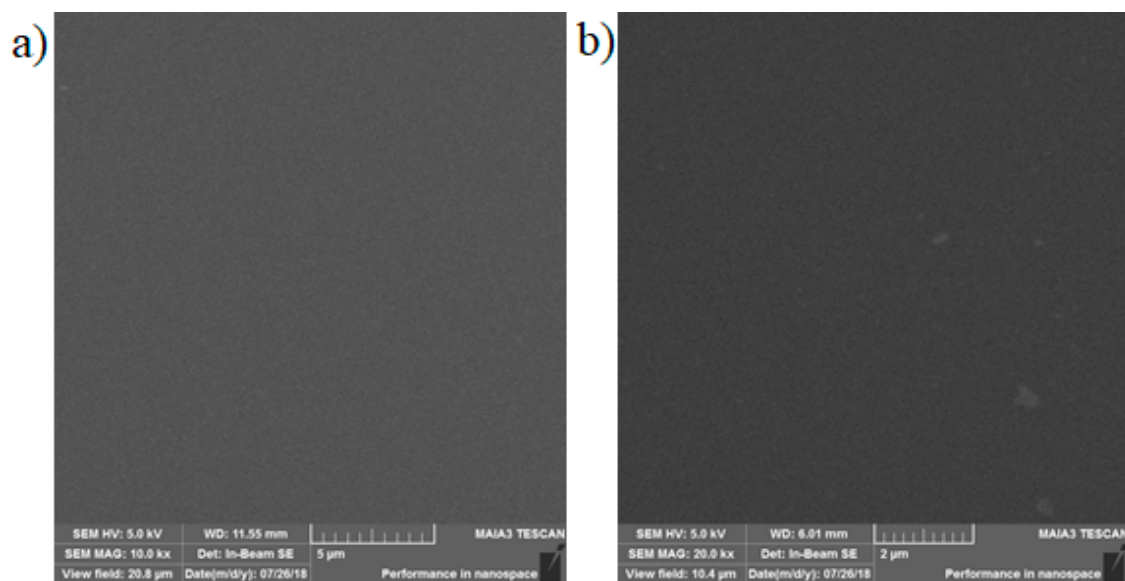


Figure S24. The SEM image of the GC electrode before and after CA.

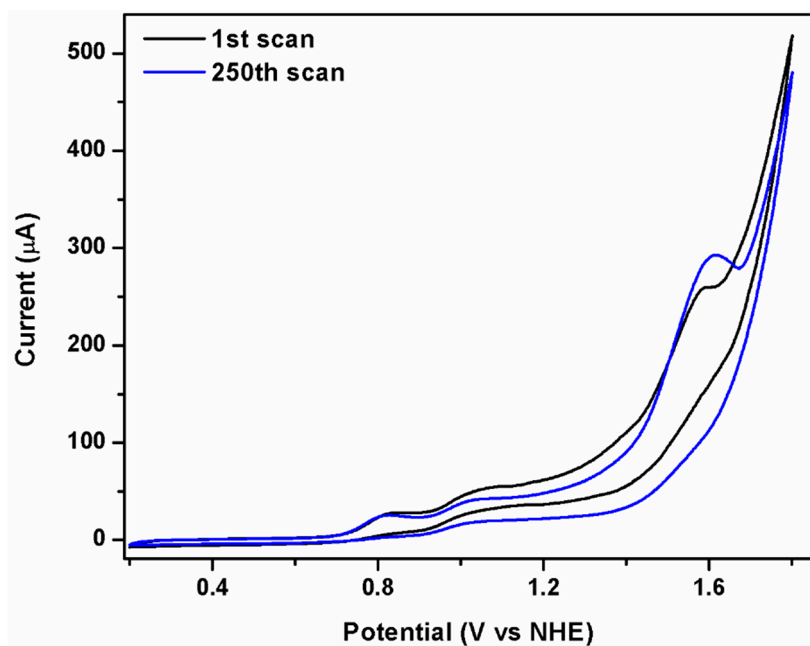


Figure S25. Successive CVs of 1.0 mM $\text{Na}_3[\text{Ru}_2(\mu\text{-CO}_3)_4]$ in 0.10 M NaHCO_3 (pH 8.3) at a scan rate of 50 mV s^{-1} .

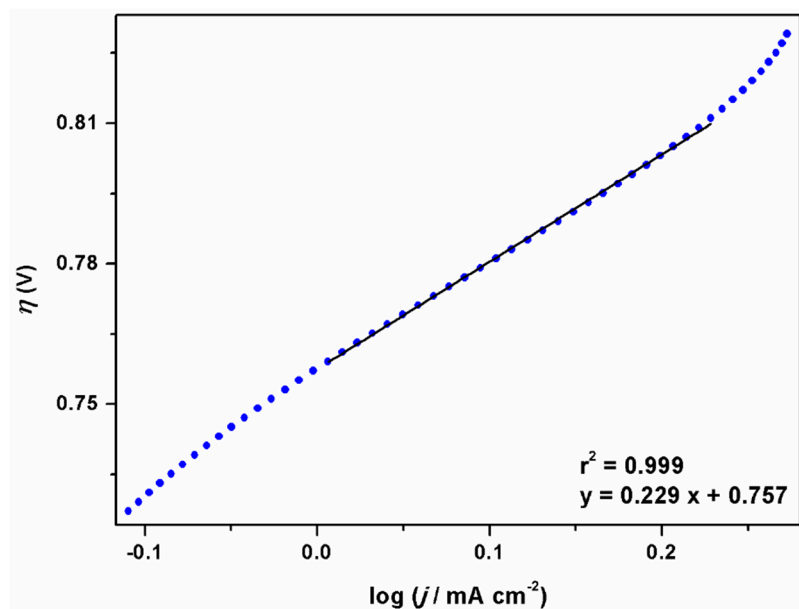


Figure S26. Tafel plot in presence of bicarbonate. LSV is recorded in 1.0 mM $\text{Na}_3[\text{Ru}_2(\mu\text{-CO}_3)_4]$ in 0.10 M NaHCO_3 at pH 8.3 at a scan rate of 50 mV s^{-1} .

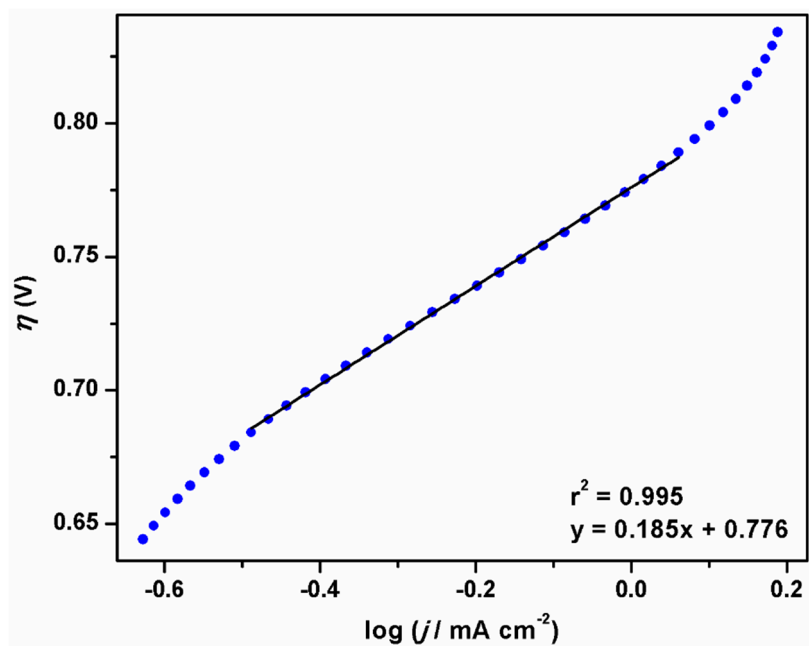


Figure S27. Tafel plot under neutral condition. LSV is recorded in a solution containing 1.0 mM $\text{Na}_3[\text{Ru}_2(\mu\text{-CO}_3)_4]$ in 0.20 M NaClO_4 at pH 7.0 at a scan rate of 50 mV s^{-1} .

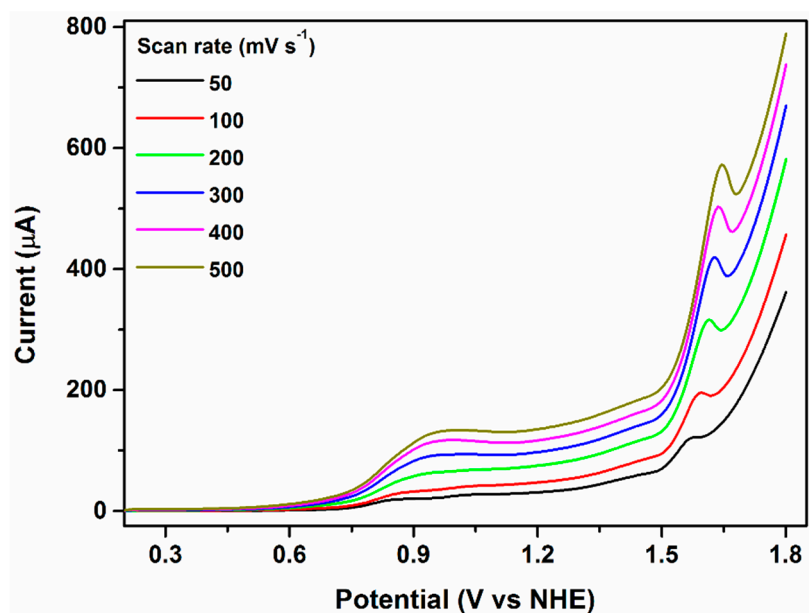


Figure S28. CVs of 1.0 mM $\text{Na}_3[\text{Ru}_2(\mu\text{-CO}_3)_4]$ in 0.10 M NaHCO_3 at pH 8.3 at various scan rates.

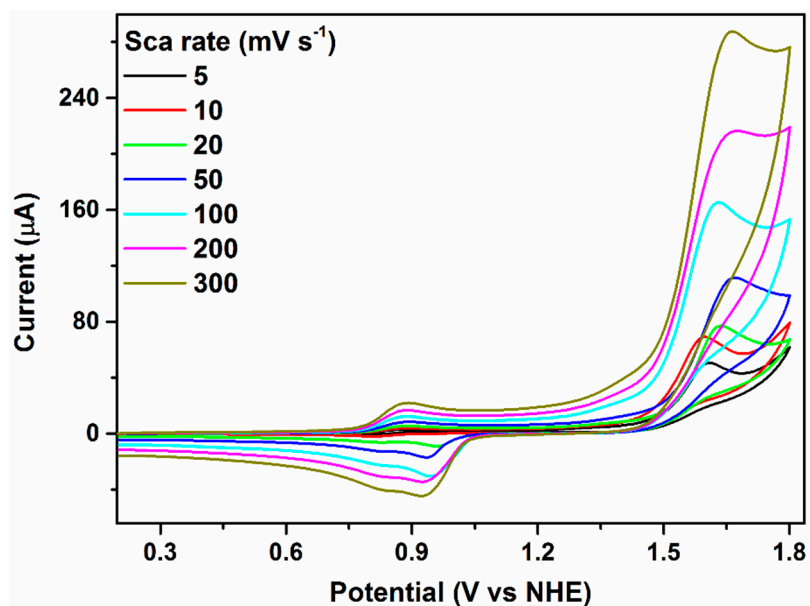


Figure S29. CVs of 1.0 mM $\text{Na}_3[\text{Ru}_2(\mu\text{-CO}_3)_4]$ in 0.20 M NaClO_4 at pH 7.0 at various scan rates.

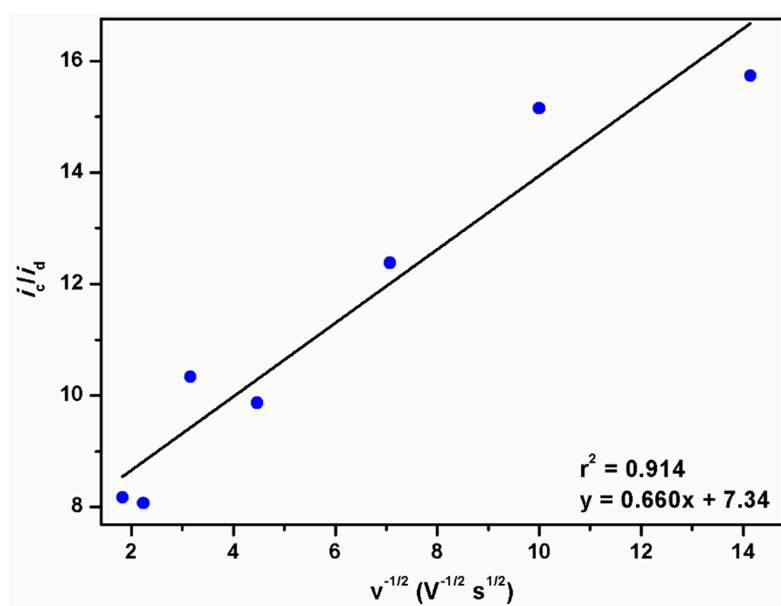


Figure S30. A Plot of i_c/i_a vs $v^{-1/2}$ for a solution containing 1.0 mM $\text{Na}_3[\text{Ru}_2(\mu\text{-CO}_3)_4]$ in 0.20 M NaClO_4 (pH 7.0). The i_c is taken at 1.56 V.